https://doi.org/10.1016/j.tws.2022.110174

Investigations into the local buckling and post-buckling behaviour of fixed-ended hybrid I-section stub columns with slender web

Shuxian CHEN[1]; Jun-zhi LIU[2]; Tak-Ming CHAN[1]*

1 Department of Civil and Environmental Engineering, The Hong Kong Polytechnic University, Hong Kong, China

2 School of National Safety and Emergency Management, Beijing Normal University, China. (Formerly, Department of Civil and Environmental Engineering, The Hong Kong Polytechnic University, Hong Kong, China)

* Corresponding author: tak-ming.chan@polyu.edu.hk

Abstract

It has been known that thin plate can carry loads considerably more than the buckling loads. This phenomenon is defined as the post-buckling behaviour, which is affected by material properties, geometric dimensions and boundary conditions of the plate. Hybrid I-section is a design concept where flanges are made of high strength steel and web is made of lower steel grade. In order to investigate the effect of slender web on the local buckling and post buckling of hybrid I-section under pure compression, experimental studies of twelve fixed-ended I-section stub columns with slender web were conducted. Tensile coupon tests and initial local geometric imperfection measurement were carried out before stub column tests. Experimental and theoretical methods for determining the critical local buckling load of plate elements were discussed, followed by a post-test finite element analysis to investigate the effects of stub column length and sectional steel combination on the buckling behaviour. Based on the

experimental and numerical results, it was observed that for specimens which web plate failed by elastic local buckling, the ultimate test loads are affected by the web strength grade, indicating that the unbuckled portion of slender web plate still provides the post-buckling strength for I-section stub columns even after yielding. By comparing the existing design methods with the numerical ultimate loads, it was found that the Eurocode 3 gives the less scattered predictions than the North American code, Australian code and Chinese code, as well as the existing direct strength method and continuous strength method.

Keywords: Local buckling; post buckling; hybrid I-section; slender web; stub column.

1 Introduction

High strength steel (HSS), typically defined as the steel with nominal yield strength of more than 460 MPa [1] has attracted increasing attention in the engineering construction because of its higher strength-to-weight ratio. Hybrid I-section is a design concept in which flange plates are made of HSS, but lower strength steel is used for the web plate. The limited contribution of the web plate for the I-section under bending makes hybrid I-beams to be a more economical alternative than homogeneous HSS I-sections [2]. The studies on the bending behaviour of hybrid I-section flexural members have emerged since the 2000s. By comparing the bending behaviour between three hybrid I-beams and their homogeneous HSS counterparts under three-point bending, Ito et al. [3] observed that the extent of web yielding region in hybrid I-section is larger, and the difference of rotation capacity between hybrid and homogeneous girders tends to increase with the increment of web slenderness. Shokouhian and Shi [4] also explored the

flexural strength of hybrid steel I-beams by tests, it was stated by authors that the web slenderness affects the local buckling failure mode of hybrid I-sections (flange local buckling, web local buckling or interactive flange-web buckling). To understand flexural behaviour and ductility of high performance steel girders, Wang et al. [5] carried out eighteen full-scale bending tests, it was found that different size of web buckling field occurs in I-sections made of different web steel, and an optimized material matching between flange and web needs to be sought.

There have not yet been extensive studies of the compressive behaviour of hybrid I-section stub columns, as it was argued that the plate elements of hybrid I-section under pure compression experience the same axial stress before yielding and local buckling. However, it is noteworthy that the thin plate can carry loads considerably more than the buckling loads. This phenomenon is called as the post-buckling behaviour, which has been proved to be relevant to the material properties, geometric dimensions, and boundary conditions of the plate [6]. In this research, slender web, whose local buckling is expected to be occurred in the elastic range, is taken as the main concern to study the local buckling and post buckling behaviour of hybrid I-sections under pure compression. The research outcomes on stub columns are fundamental to help understand the cross-section behaviour of hybrid I-sections subject to the complex loading scenarios.

To this end, experimental studies of twelve fixed-ended I-section stub columns with slender web were carried out. Among them, eight test specimens are hybrid sections, and the remaining four are homogeneous HSS counterparts designed for comparison. Tensile coupon tests and initial local imperfection measurements were conducted before stub column tests. The failure

mode of test specimens is presented, the critical local buckling loads of plate elements obtained through experimental methods and theoretical methods are discussed, and the ultimate test loads of I-section stub columns are studied. Furthermore, a post-test finite element analysis was performed to investigate the effects of stub column length and sectional steel combination on the local buckling and post buckling behaviour of I-sections with slender web. Besides, the design approaches adopted in the current European, North American, Australian, and Chinese codes of steel structures, as well as the existing direct strength method (DSM) [7] and continuous strength method (CSM) [8] are assessed.

2 Test programme

2.1 Test specimens

Twelve I-section stub columns fabricated by 10 mm thick flanges and 6 mm thick web were tested in this research. Chinese steel Q690 (nominal yield strength $f_{y,\,nom}$ = 690 MPa), labelled as "Q690-F", was selected to be the flange plate of all the I-sections, while three steel strength grades: "Q690-W", "Q460" ($f_{y,\,nom}$ = 460 MPa) and "Q355" ($f_{y,\,nom}$ = 355 MPa) were used as the web plates to examine the effect of web materials on the local buckling and post-buckling behaviour of I-section stub columns with slender web. Three sectional steel combinations were selected for test specimens: (1) Q690 flange and Q690 web; (2) Q690 flange and Q460 web; (3) Q690 flange and Q355 web. Among them, combination (1) can be taken as the benchmarked homogeneous section.

The nomenclature of I-shaped cross-section is shown in **Fig. 1**. In this figure, b_f and t_f are the width and thickness of flange; H and h_w denote the section height and the clear distance

between flanges; t_w is the thickness of web plate. The flange and web plates of I-sections are joined by 6 mm thick fillet weld, and the welding process was executed manually using gas metal arc welding (GMAW) with a gas mixture of 80% Argon and 20% carbon dioxide.

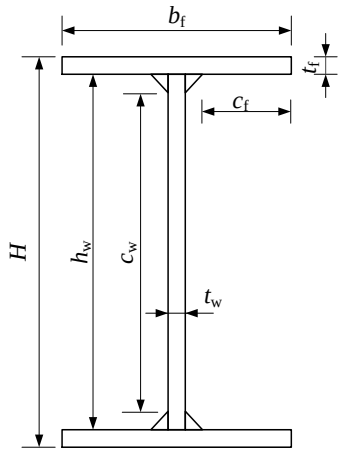

Figure 1. Nomenclature of I-shaped cross-section

As shown in **Table 1**, three test series-"H230", "H350" and "H440" were designed to be characterised with 230 mm, 350 mm and 440 mm section height to be with slender web and to achieve a wide range of web slenderness. The slender web limit under compression in North American code [9], as expressed by Equation (1), was adopted in this research. As mentioned before, three web steel materials "Q690-W", "Q460" and "Q355" were used for each series.

$$h_w / t_w \geq 1.49 \times \sqrt{\frac{E}{f_{yw}}} \tag{1}$$

Table 1. Nominal dimensions of fixed-ended I-section stub columns with slender web

Series	b_f (mm)	t_f (mm)	H (mm)	h_w (mm)	t_w (mm)	L (mm)	Number
H230-web steel-L1	110	10	230	210	6	255	3
H230-web steel-L2						465	3

H350-web steel	350	330		400	3
H440-web steel	440	420		500	3

In addition, it has been known the recently developed design approaches - the direct strength method (DSM) and continuous strength method (CSM), are based on the overall cross-section slenderness λ_p instead of the slenderness of individual constitutive plates, for considering the flange-web interaction. The expression of λ_p for compression member is indicated by Equation (2).

$$\lambda_p = \sqrt{\frac{N_y}{\sigma_{cr,cs} \times A_{cs}}} \tag{2}$$

$$N_y = f_{yf} \times A_f + f_{yw} \times A_w \tag{3}$$

$$A_{cs} = A_f + A_w \tag{4}$$

where, N_y denotes the yield load of the whole section (Equation (3)); $\sigma_{cr,cs}$ represents the critical elastic local buckling stress of full cross-section, and A_{cs} is the sectional area (Equation (4)). In Equation (3), A_w and σ_{yw} are the area and yield strength of web plate, A_f and σ_{yf} are defined as the gross area and yield strength of flanges. As for $\sigma_{cr,cs}$, it can be determined by numerical methods or empirical estimation formulae. The prediction approach established by Gardner et al. [10] was adopted in this research. In their method, the elastic buckling stresses of the isolated web and flange with simply supported and fixed boundary conditions are firstly determined by the classic plate buckling theory [11], and then an interaction coefficient ζ, whose formulae are underpinned by the statistical results of finite strip analyses, is adopted to quantify the degree of element interaction. The expression of ζ is dependent on the cross-section geometry and the stress state across the section.

For the selection of stub column length L, it has been widely accepted that a length of at least three times the width of the widest plate element (namely, h_w in this research) should be ensured [11]. However, this rule may not be suitable for slender web I-sections studied in this research, as the column with length of $3h_w$ may prone to global flexural buckling. To address this issue, a preliminary finite element analysis was conducted before selecting the stub column length. The numerical results indicate that 1.2 times the compressed edge width of web plate ($1.2h_w$) is acceptable to make sure all these web-critical I-sections failed by local buckling with one nominal half-wave length [12]. As a result, $1.2h_w$ (L1) was adopted for stub columns except for "H230" series, for which 2.2 times the compressed web plate edge (L2) was also considered to explore the effect of stub column length L on the compressive resistance of I-section stub columns. A detailed discussion on the length effect is presented in Section 4.2 by means of finite element analysis.

Table 2 provides the measured geometric characteristics of all the test specimens, as well as the North American code slender limit for web plate and overall cross-section slenderness. Seen from **Table 2**, all the webs are defined as slender except for those of "H230-355W-L1" and "H230-355W-L2", as the web thickness of these two specimens (6.8 mm and 6.7 mm) is greater than its nominal thickness - 6mm. Also, as can be seen from the table that in one series (series "H230", "H350" or "H440"), the I-section with lowest strength web gives the least value of λ_p. This is because the value of $\sigma_{cr,cs}$ is independent of the sectional steel combination, while N_y is calculated on the yield strength of both flanges and web.

Table 2. Measured geometric characteristics of I-section stub columns with slender web

Specimen	b_f (mm)	t_f (mm)	h_w (mm)	t_w (mm)	L (mm)	Web slender limit	h_w/t_w	λ_p
H230-690W-L1	110.3	9.8	207.8	6.2	252	23.7	33.5	0.83
H230-690W-L2	110.8	9.6	208.1	6.4	462	23.7	32.5	0.82
H230-460W-L1	109.9	9.7	207.5	6.6	251	29.4	31.4	0.74
H230-460W-L2	109.8	9.6	208.7	6.6	462	29.4	31.6	0.74
H230-355W-L1	109.6	9.7	209.1	6.8	251	34.1	30.7	0.70
H230-355W-L2	110.0	9.7	209.3	6.7	462	34.1	31.2	0.71
H350-690W	109.8	9.5	329.2	6.5	400	23.7	50.6	1.29
H350-460W	110.4	9.6	330.1	6.6	396	29.4	50.0	1.16
H350-355W	110.0	9.7	329.3	6.8	396	34.1	48.4	1.07
H440-690W	110.1	9.6	420.2	6.3	499	23.7	66.3	1.68
H440-460W	109.7	9.7	420.3	6.3	500	29.4	66.8	1.53
H440-355W	110.1	9.5	419.6	6.7	499	34.1	62.8	1.36

2.2 Material properties

In accordance with EN ISO 6892-1 [13], tensile coupon tests for parent plates of I-sections were carried out through a 100 kN electromechanical universal testing machine with advanced video extensometer at Industrial Centre in The Hong Kong Polytechnic University. Two visible white dots with a distance of extensometer gauge length were marked on the outer surface of coupons so that the non-contacting device — Advanced video extensometer can easily capture the changing displacements between dots by a data acquisition rate of 490Hz, as illustrated in

Fig. 2. Three material samples were cut from each parent plate along the longitudinal direction of I-sections. The measured stress-strain curves of steel plates are displayed in **Fig. 3**, and the average measured material characteristics are presented in **Table 3**. In this table, E is the elastic modulus; ε_y, ε_{sh} and ε_u represent the yield strain, strain at the onset of strain hardening and ultimate strain; f_y and f_u mean the yield strength and ultimate strength.

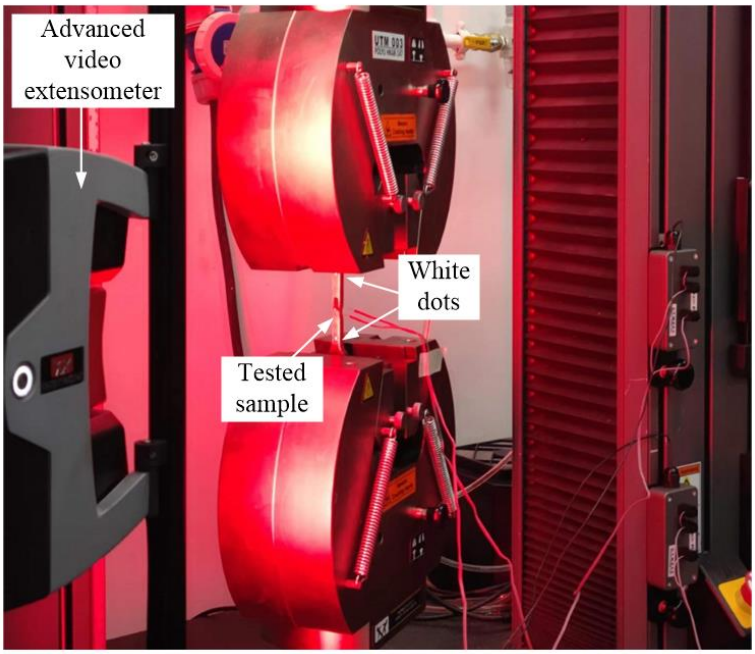

Figure 2. Setup of tensile coupon tests

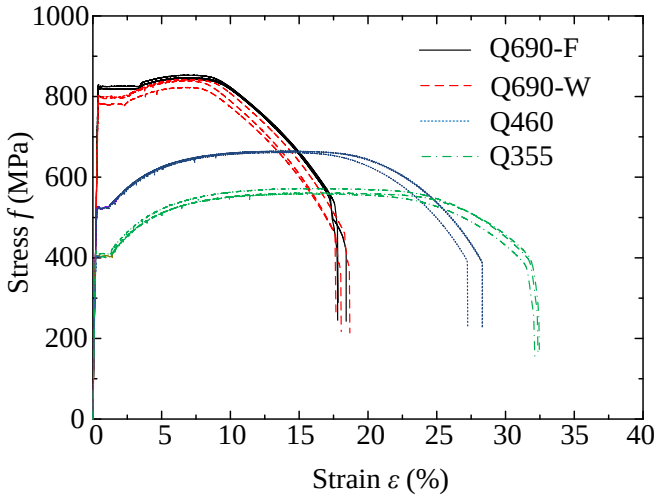

Figure 3. Measured stress-strain curves of steel materials

Table 3. Average measured material characteristics of steel materials

Steel	E (GPa)	ε_y (%)	ε_{sh} (%)	ε_u (%)	f_y (MPa)	f_u (MPa)
Q690-F	217.4	0.377	3.42	6.75	819.5	848.4
Q690-W	216.1	0.365	2.46	6.86	788.9	834.5
Q460	215.8	0.241	1.13	13.6	520.9	663.5
Q355	220.0	0.183	1.36	15.6	402.2	563.7

2.3 Initial local geometric imperfection measurement

The initial local geometric imperfection of I-section is mainly from the welding of constitutive plates, which can be simplified as the shape displayed by **Fig. 4** [14, 15]. In this figure, e_f and e_w represent the imperfection magnitudes of outstand flanges and internal web element, respectively. To capture the local imperfection, an I-section stub column was clamped onto the milling machine, and then the machine table was moved automatically so that the fixed linear variable differential transformers (LVDTs) can measure the continuous magnitudes of this specimen along the travelling direction, as displayed in **Fig. 5**. **Fig. 6** shows the arrangement of local imperfection measurement: measurement along the transverse direction in the initial position ("0") was conducted first to obtain the records at the marked points (A_0, M_0 and B_0); and then, starting from "0", three LVDTs were moved simultaneously along the longitudinal direction, so that the results at the "n" position, i.e., A_n, M_n and B_n can be obtained by adding the respective recorded readings to A_0, M_0 and B_0. Consequently, the local geometric imperfection of plates is the deviation of central line from the average magnitudes of two edge lines, as indicated by $(A_n+B_n)/2-M_n$. The measured maximum magnitude of plate elements for each I-section test specimens is summarized in **Table 4**. In this table, c_f is the distance from

flange outstand edge to weld, and c_w is the distance between welds, as shown in **Fig. 1**. It can be seen that the measured local imperfection magnitude of outstand flange is close to the one (1/50) recommended in EN 1993-1-5 [14] for finite element modelling, while for the internal web plate, the measured values are less than that (1/200) in Eurocode 3.

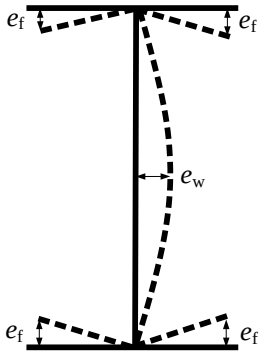

Figure 4. Diagram of initial local geometric imperfection shape for I-section

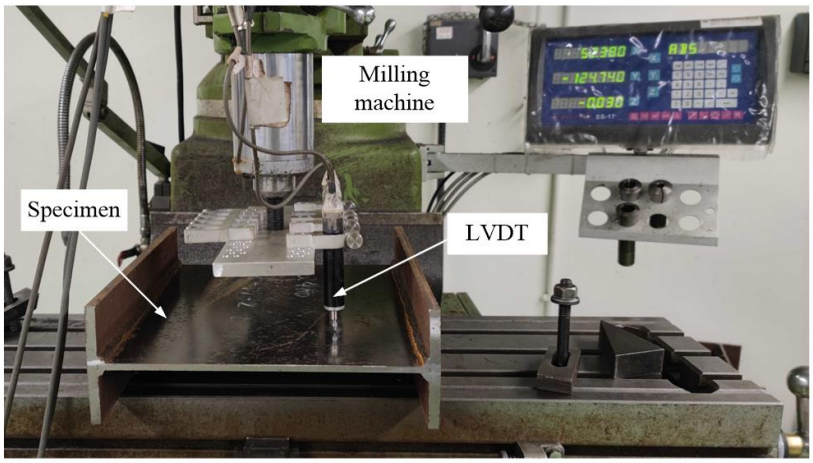

(a) Transverse direction

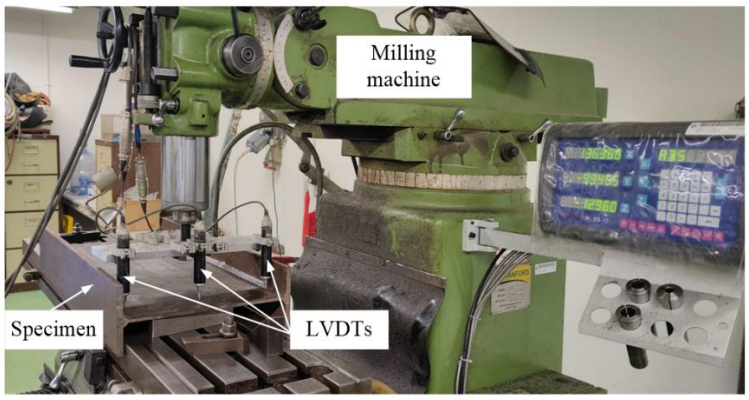

(b) Longitudinal direction

Figure 5. Setup of local geometric imperfection measurement

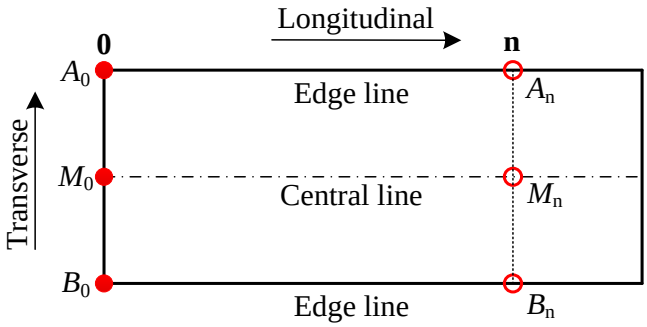

Figure 6. Arrangement of local imperfection measurement for the plate element in I-section

Table 4. Measured initial local geometric imperfection of test specimens

Specimen	e_f (mm)	e_f/c_f	e_w (mm)	e_w/c_w
H230-690W-L1	0.631	1/73	0.451	1/434
H230-690W-L2	0.677	1/68	0.391	1/504
H230-460W-L1	1.225	1/37	0.522	1/375
H230-460W-L2	1.417	1/32	0.492	1/400
H230-355W-L1	1.120	1/38	0.163	1/1209
H230-355W-L2	1.159	1/39	0.292	1/676
H350-690W	0.562	1/81	0.162	1/1958
H350-460W	1.094	1/42	0.274	1/1161
H350-355W	1.091	1/42	0.349	1/909
H440-690W	1.009	1/45	0.649	1/629
H440-460W	1.034	1/44	0.610	1/669
H440-355W	1.158	1/39	0.462	1/882
Mean		1/49		1/817

195 **2.4 Stub column test setup**

196 All the specimens were milled flat at both ends before testing to ensure the compressive load
197 is distributed uniformly on the cross-section. The stub column tests were conducted by either
198 a 4600 kN hydraulic testing machine or a 25000 kN universal servo-controlled testing machine
199 at The Hong Kong Polytechnic University. **Fig. 7(a)** shows the stub column test setup. The
200 central lines of the tested specimen, loading plate and bearing plate were marked carefully prior
201 to centring, tested specimen was then aligned between the loading and bearing plates using the
202 vertical line projected by high-precision self-levelling rotary laser level placed in the both front
203 and lateral sides of the test machine, as shown in **Fig. 7(b)**; the rigid jig with tightened high-
204 strength bolts was mounted at each end of specimen to avoid the occurrence of premature local
205 buckling; four LVDTs were arranged at the four corners to capture the end shortening of
206 specimen. The instrumentation configuration of stub column tests was illustrated in **Fig. 7(c)**.
207 In this figure, "A-A" is the section at the mid-length of stub column, where electrical strain
208 gauges were symmetrically placed on the outer surface of flanges and both sides of web plate,
209 and "B-B" section is the one at the end of test specimen, showing the outline of the rigid jig
210 clearly. The compression tests of I-section stub columns were performed with a rate of
211 0.5mm/min until the load drops to 80% ultimate value N_u.

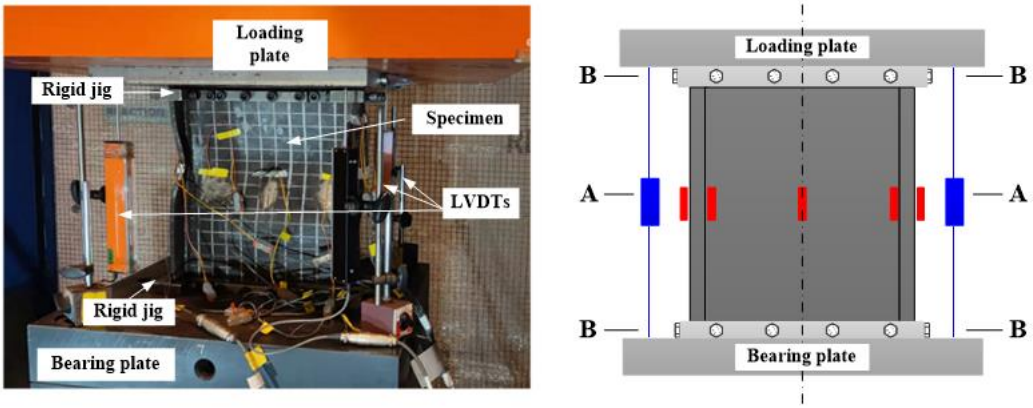

(a) Stub column test setup

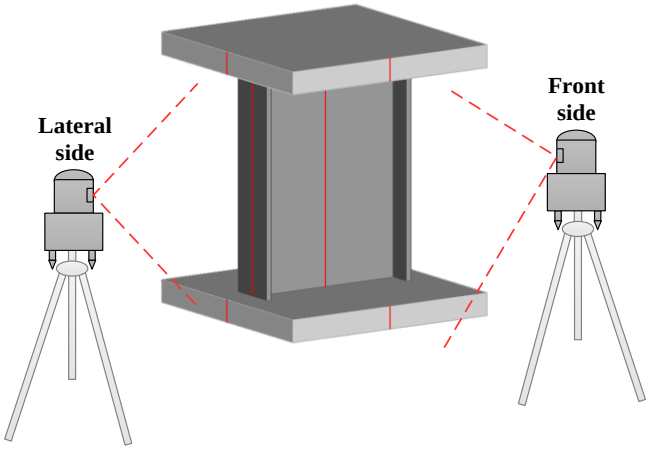

(b) Centring of stub column

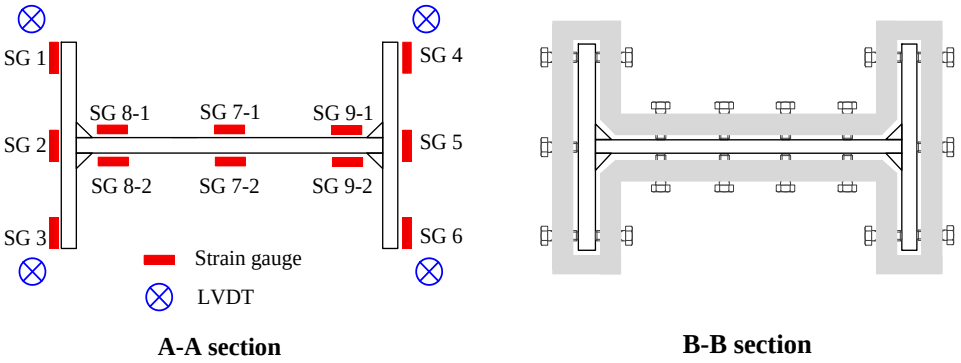

(c) Instrumentations

Figure 7. Stub column test setup with instrumentation configurations

3. Test results

3.1 Failure mode

The deformed shape of twelve fixed-ended I-section stub columns with slender web is shown in **Fig. 8**. As anticipated, all the test specimens failed due to the occurrence of local buckling, and the deformation mainly locates at the mid-length of columns. **Fig. 9** presents the axial load N-end shortening δ_e curve of specimens, all of which show the typical load-deformation behaviour of stub columns with slender cross-section [16].

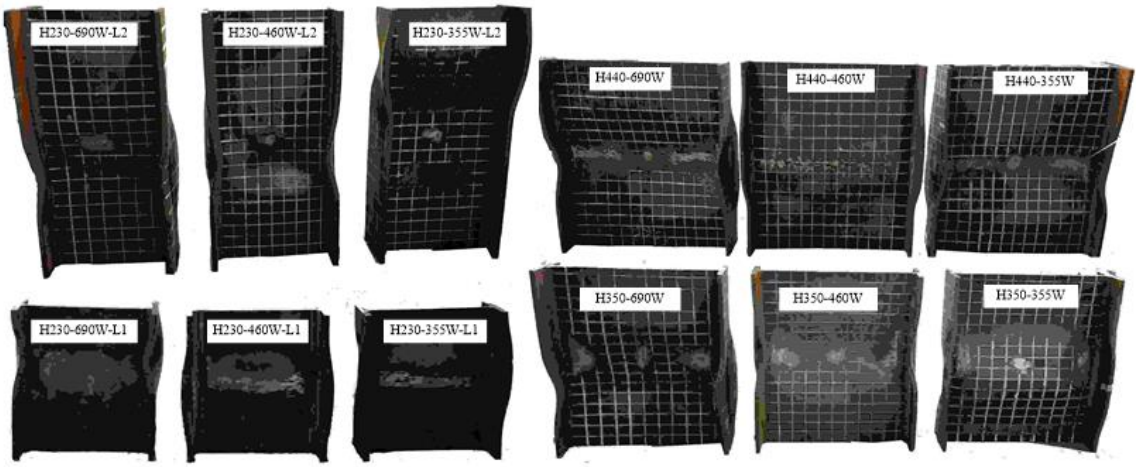

Figure 8. Failure mode of test specimens

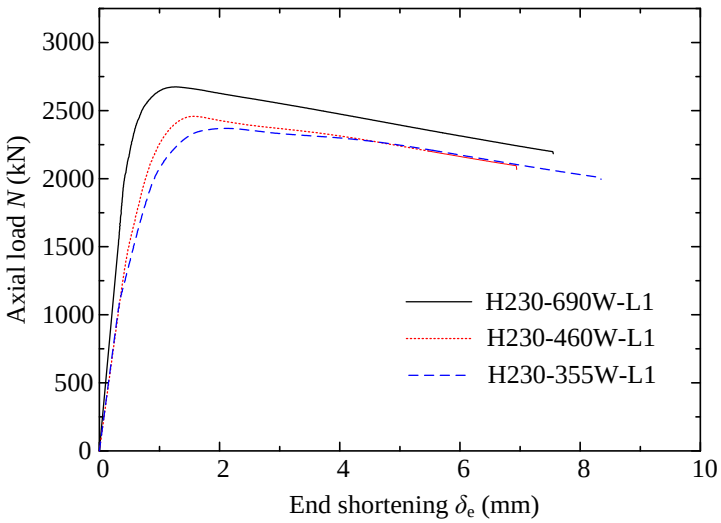

(a) "H230-L1" series

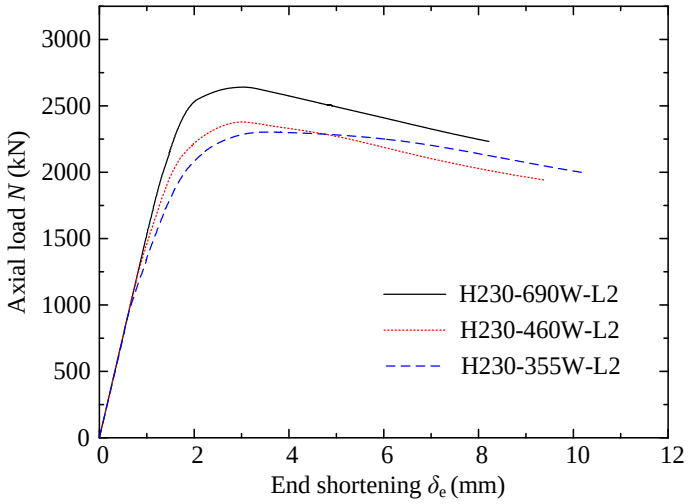

233

234 (b) “H230-L2” series

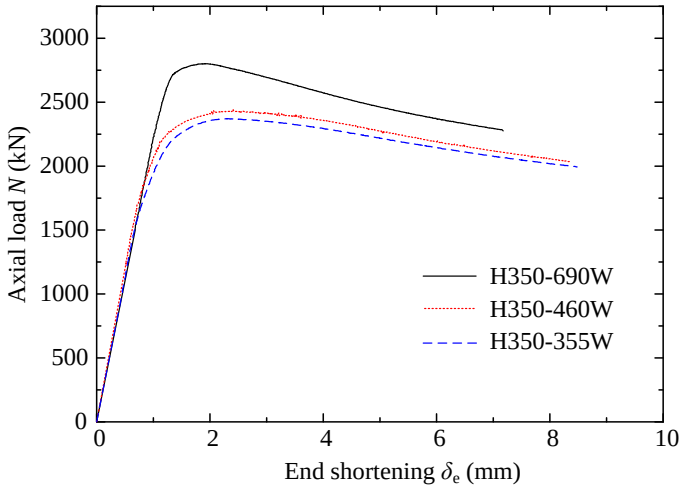

235

236 (c) “H350” series

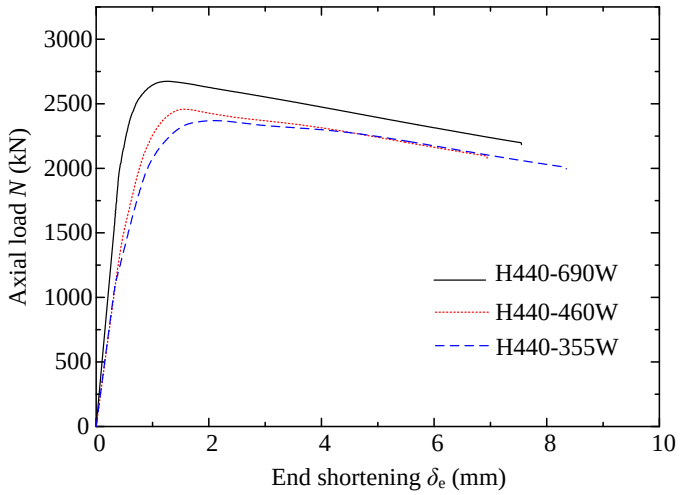

237

238 (d) “H440” series

Figure 9. Axial load-end shortening curves of test specimens

3.2 Critical local buckling load

In order to study the effect of web strength grade on the local buckling and post buckling behaviour of hybrid I-section stub columns with slender web, a discussion on the critical local buckling of plate elements for test specimens is presented in the subsequent sections.

3.2.1 Experimental methods

The determination of critical load on plate buckling by test data has been addressed in the past [6, 17, 18]. In this research, both the direct and indirect strain-dependent experimental methods were applied to evaluate the critical local buckling load for plate elements.

The direct methods include the strain reversal method, average strain method and bending strain method. The average strain ε_a and bending strain ε_b of one plate can be calculated based on the paired strain gauges applied on opposite side of the plate where the measured strains on the concave side and convex side are ε_1 and ε_2 respectively. ε_a and ε_b are then expressed by Equations (5) and (6), respectively.

$$\varepsilon_a = \frac{\varepsilon_1 + \varepsilon_2}{2} \tag{5}$$

$$\varepsilon_b = \frac{\varepsilon_1 - \varepsilon_2}{2} \tag{6}$$

In the strain reversal method [19], the critical load N_{cr} is defined as the load where the surface strain on the convex side of plate begins to present the opposite increasing trend as a turning point. For the average strain method [20], N_{cr} is the point where a sharp break appears in the load-average strain curve. In the load-bending strain curve [21], this plate buckling load can be determined by the inflection point or the extrapolation of curve beyond buckling.

In this research, the critical local buckling load of flange plate $N_{cr,f}$ for test specimens was obtained by the strain reversal method. The comparison between flange critical loads $N_{cr,f}$ and ultimate loads of test specimens $N_{u.test}$ is presented in **Table 5**. It is evident that the flange critical load $N_{cr,f}$ of all the specimens is extremely close to the ultimate test load $N_{u,test}$, indicating that the decrease in axial load capacity of I-section stub columns stems from the local buckling of flanges.

The critical load of web plate $N_{cr,w}$ could be derived through all the above mentioned direct experimental methods—the strain reversal method, average strain method and bending strain method. The ratios of web critical loads $N_{cr,w}$ by different direct methods to ultimate test loads $N_{u.test}$ are given in **Table 5**, where "-" means the web critical load $N_{cr,w}$ of this specimen is unable to be determined by the average strain method. The load-strain curves of specimens "H230-460W-L1", "H350-690W", "H440-460W" and "H440-355W" are presented in **Figure 10** as the representative examples to determine the critical local buckling load $N_{cr,w}$ for web plate, and the red dots in this figure signify the critical loads $N_{cr,w}$ obtained by different direct strain-dependent methods.

Table 5. Comparison of ultimate loads with critical local buckling loads of plate elements determined by direct strain-dependent experimental methods

Specimen	$N_{cr,f}/N_{u,test}$	$N_{cr,w}/N_{u,test}$		
	Strain reversal method`	Strain reversal method	Axial strain method	Bending strain method
H230-690W-L1	1.00	0.79	0.75	0.74
H230-690W-L2	0.98	0.93	0.94	0.92
H230-460W-L1	0.99	0.96	-	0.86
H230-460W-L2	0.98	0.93	-	0.93
H230-355W-L1	1.00	1.00	-	0.95
H230-355W-L2	0.99	0.87	-	0.93
H350-690W	0.99	0.66	0.83	0.65
H350-460W	0.91	0.58	0.69	0.56
H350-355W	0.98	0.68	0.70	0.67
H440-690W	0.95	0.34	-	0.34
H440-460W	0.99	0.42	-	0.43
H440-355W	0.97	0.43	0.57	0.63

The cases of "H230-460W-L1" and "H440-460W" specimens are displayed in **Fig. 10(a) and 10(c),** where no obvious sharp break is observed in their load-average strain curves. For "H350-690W" specimen shown in **Fig. 10(b)**, the results of $N_{cr,w}$ determined by the average strain method is greater than those through the strain reversal method and bending strain method, while the web critical load $N_{cr,w}$ of "H440-355W" specimen (**Fig. 10(d)**) via the strain reversal

method is slightly less than the other two methods. In addition, a significant observation is that the web critical load $N_{cr,w}$ of "H350" and "H440" series is much less than the ultimate load $N_{u,test}$, indicating the existence of post-buckling strength for the web plate, which is provided by the restraint of joined flanges.

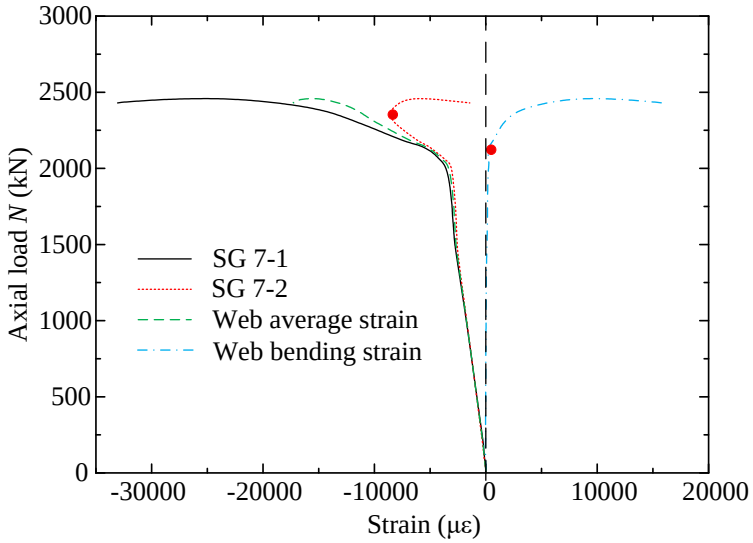

(a) H230-460W-L1

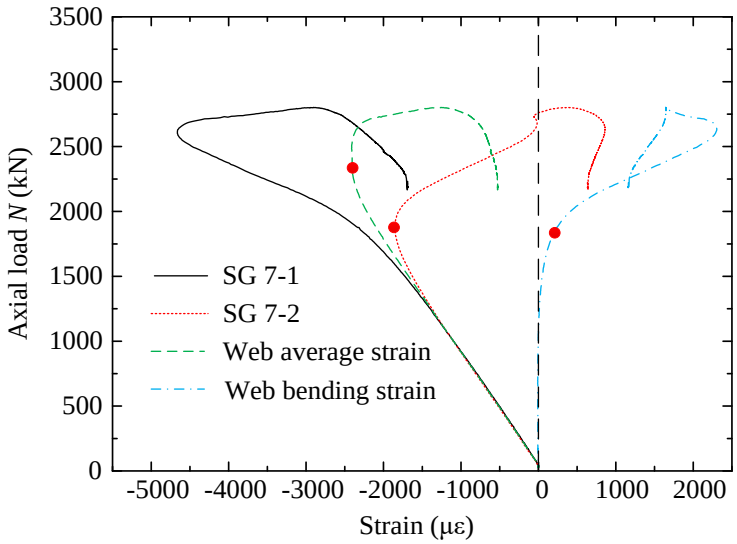

(b) H350-690W

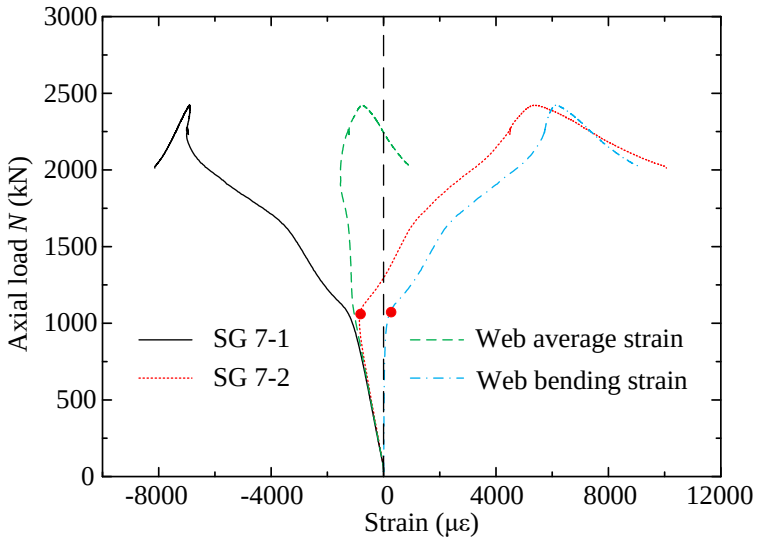

(c) H440-460W

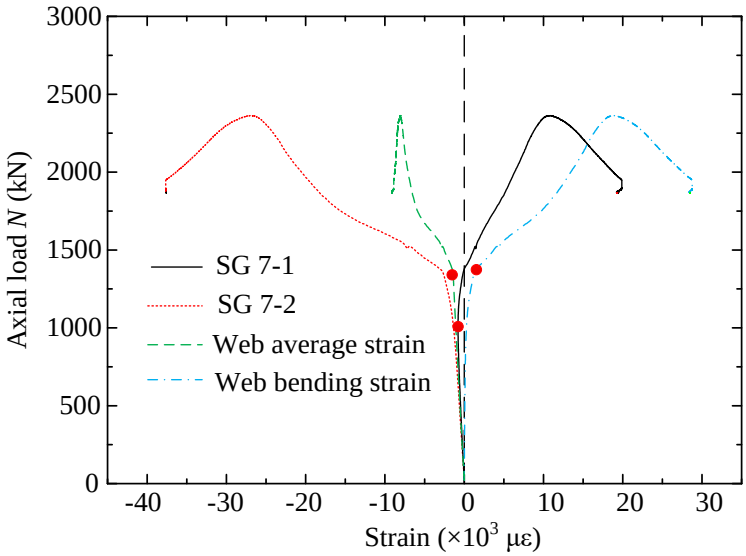

(d) H440-355W

Figure 10. Determination of the critical local buckling load for web plate $N_{cr,w}$ by direct strain-dependent experimental methods

Furthermore, the applicability of indirect experimental methods, which can describe the post-buckling behaviour of plate, is discussed. One of the indirect methods is the Modified Southwell method proposed by Barbero and Trovillion [22] by extending the widely used

Southwell method [23]. Note that the nature of Southwell method is based on the neutral characteristics which excludes the possibility of any post-buckling behaviour [6]. To overcome this limitation, Barbero and Trovillion [22] established the Modified Southwell method by approximating the post-buckling path of plate as quadratic curve, so that the critical local buckling load N_{cr} of plate can be obtained by Equation (7).

$$N = N_{cr} + \frac{1}{2} \times N^{(2)} \times s \tag{7}$$

where, s is the perturbation parameter; $N^{(2)}$ is the curvature of the post-buckling path, whose value is a constant in the quadratic curve.

Another indirect experimental method is the Koiter method [24], which has been utilized to predict the critical load of composite columns with pronounced post-buckling behaviour in the last decade [25-27]. It was stated that the expression of the Koiter method, as indicated by Equation (8), is able to represent the initial post-buckling path near critical load of structures [28].

$$N = N_{cr} \times \frac{1 + c_1 \times (s - b) + c_2 \times (s - b)^2}{1 + s_0 / (s - b)} \tag{8}$$

where, c_1, c_2 and b are the constants to be determined; s_0 is initial imperfection. Under the situation of the plate under compression, the value of c_1 can be taken as zero [29].

In this research, the bending strain ε_b is regarded as the perturbation parameter s in the Modified Southwell method and Koiter method. By the regression analysis of initial post-buckling path for the web plate of test specimens, the web critical local buckling load $N_{cr,w}$ are calculated by Equations (7) and (8), Taking “H230-L1-460W”, “H330-460W” and “H440-690W” as examples, **Fig. 11** illustrates the determination of web critical local buckling loads using the Modified Southwell method and Koiter method. In this figure, the dash lines in the figure

represent the curves of Equations (7) or (8), while the solid lines are from experimental data. The results of web buckling load $N_{cr,w}$ for test specimens obtained through the Modified Southwell method and Koiter method are tabulated in **Table 6.** For comparison, the results from the bending strain method are also presented in the table. It can be seen that the above two indirect experimental methods make the similar estimations for the web critical load $N_{cr,w}$, while the results from the bending strain methods are always lesser.

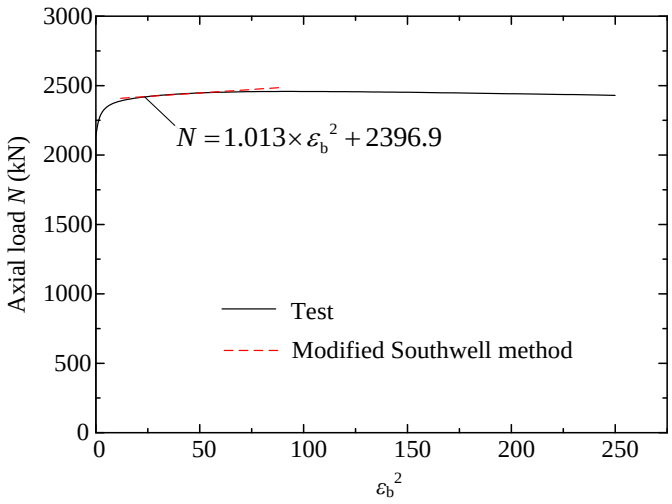

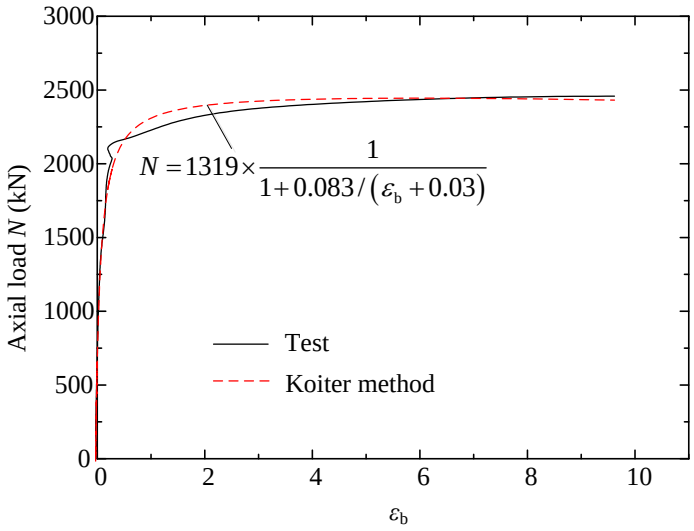

(1) H230-L1-460W

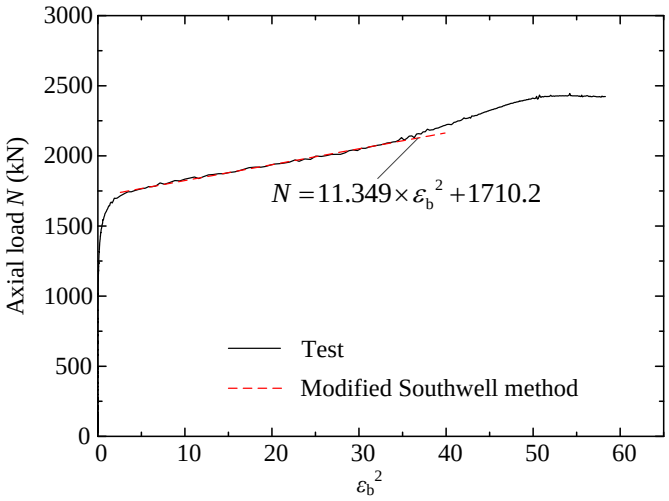

340

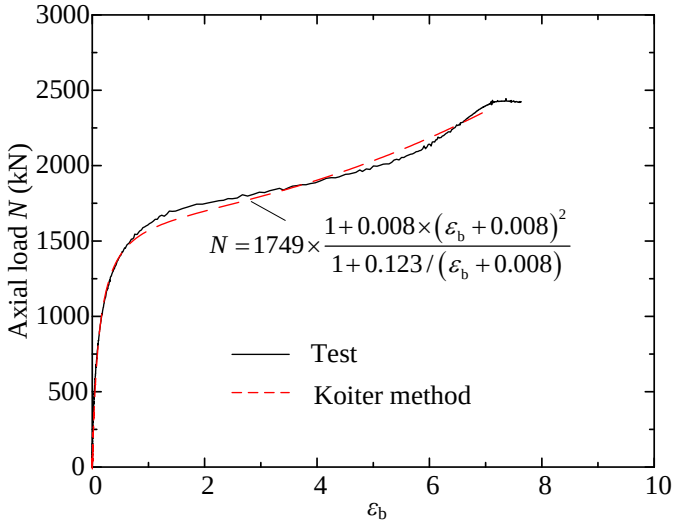

341

342 (2) H330-460W

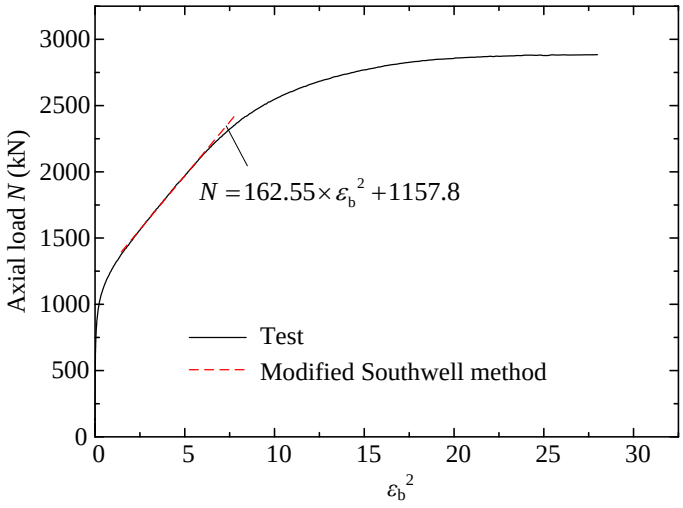

343

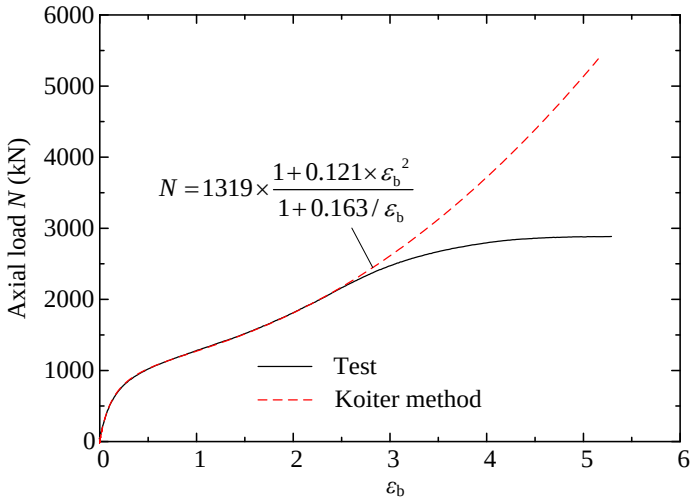

(3) H440-690W

Figure 11. Determination of the critical local buckling load for web plate $N_{cr,w}$ by indirect strain-dependent experimental methods

3.2.2 Theoretical methods

The theoretical methods for predicting the elastic critical local buckling load of plate are also explored in this research. It is well known that the elastic critical stress of plate $f_{cr,e}$ is given by Equation (9). Where, k is the buckling coefficient depending on the boundary condition and geometry of plates; υ is the Poisson's ratio of material; t and b_p are the plate's thickness and width.

$$f_{cr,e} = \frac{k\pi^2 E}{12\left(1-\nu^2\right)} \times \left(\frac{t}{b_p}\right)^2 \tag{9}$$

In the classical plate buckling theory [12], the values of k for the web are equal to 4.0 and 6.97 when the unloaded edges are simply supported and clamped, respectively. However, the restraint of web plate provided by the joined flanges in I-sections is neither ideal simply supported nor clamped, which depends on the dimension of plate elements [30]. Thus, Bleich

[31] established the formulae of buckling coefficient k for the web plate in I-sections, as expressed by Equations (10) and (11), to consider the interactive effect of flanges and web.

$$k=\left(2+\frac{2}{10\xi+3}\right)^2 \tag{10}$$

where,

$$\xi=\left(\frac{t_w}{t_f}\right)^3 \frac{0.16+0.0056\times\left(\left(H-t_w\right)/\left(b_f/2\right)\right)^2}{1-9.4\times\left(t_w/t_f\right)^2\times\left(\left(b_f/2\right)/\left(H-t_w\right)\right)^2} \tag{11}$$

The comparison of ultimate test loads $N_{u,test}$ with the prediction of theoretical methods based on the above three boundary condition is shown in **Table 6**. It is clear that the results from Bleich's equation are between those determined by the simply supported and clamped edges. For the test specimens with 230 mm section height, the elastic local buckling loads of web plate through theoretical methods are much greater than the ones from the experimental methods, implying that it is inelastic local buckling that appears in the web plate of "H230" series test specimens. Whilst the elastic local buckling loads by Bleich's equation for the other specimens, i.e., "H350" and "H440" series, are near the results from the Modified Southwell method and Koiter method. This observation verifies the applicability of Bleich's proposal for the I-section stub columns with slender web tested in this research.

Table 6. Comparison of critical local buckling loads of web plate $N_{cr,w}$ determined by experimental methods and theoretical methods with ultimate test loads $N_{u,test}$

Specimen	$N_{cr,w}/N_{u,test}$					
	Experimental methods			Theoretical methods		
	Bending strain method	Modified Southwell method	Koiter method	Simply-supported	Clamped	Bleich's equation
H230-690W-L1	0.74	0.91	0.93	1.01	1.75	1.42
H230-690W-L2	0.92	0.97	0.99	1.05	2.02	1.59
H230-460W-L1	0.86	0.98	1.02	1.09	1.89	1.53
H230-460W-L2	0.93	0.98	1.03	1.09	1.90	1.53
H230-355W-L1	0.95	1.00	1.00	1.37	2.39	1.86
H230-355W-L2	0.93	0.96	1.04	1.36	2.37	1.86
H350-690W	0.65	0.77	0.78	0.49	0.86	0.69
H350-460W	0.56	0.72	0.70	0.48	0.84	0.69
H350-	0.67	0.93	0.88	0.65	1.14	0.91

355W						
H440-690W	0.34	0.40	0.46	0.31	0.54	0.44
H440-460W	0.43	0.47	0.52	0.36	0.63	0.51
H440-355W	0.63	0.63	0.64	0.43	0.75	0.59

383

384 **3.2.3 Summary**

385 Based on the above evaluation on web critical local buckling loads by various strain-dependent
386 experimental methods and theoretical methods, it can be summarized that,

387 (1) the average strain method is unsuitable for evaluating the critical local buckling load of web
388 plate. A possible explanation for this might be that the essence of average strain method
389 (Equation (5)) makes itself more insensitive to the variation of strain on the surface of concave
390 and convex sides;

391 (2) For the slender web studied in this research, the critical local buckling load by direct
392 experimental methods (the strain reversal method, the average strain method and the bending
393 strain method) always less than those from indirect experimental methods-Modified Southwell
394 method and Koiter method;

395 (3) The web plates of "H230" series test specimens experience inelastic local buckling, while
396 it is elastic local buckling that occurs in the web of "H350" and "H440" series.

397 (4) For web plates failed by elastic local buckling, it is suggested to adopt Modified Southwell
398 method and Koiter method if test data are available, otherwise the Bleich's formula could be

used to evaluate the critical elastic local buckling load.

3.3 Ultimate load

Ultimate loads of test specimens are presented in **Table 7**, with comparison of the derived yield load N_y. It was found in this table that the ultimate loads of "H230" series nearly reach or exceed the yield load, which accords with the earlier observation in Section 3.2.2 on the occurrence of inelastic local buckling for specimens with 230 mm section height.

In addition, as mentioned before, the web plates of series "H350" and "H440" test specimens experience web elastic local buckling, which is thought to be related to the plate dimension only (aside from elastic modulus E and Poisson's ratio υ). However, seen from the comparison of ultimate loads among three specimens in one series in **Table 7**, the steel grade of web plate still plays a non-negligible role in the compressive strength of the whole section. For example, the ultimate load of "H350-690W" (2802 kN) is fairly greater than those of "H350-460W" (2445 kN) and "H350-355W" (2371 kN).

In addition, by comparing the ultimate test loads of specimens with nominally identical material and section properties but different column length (L1 and L2), it can be concluded from **Table 7** that the stub column length plays a negligible role in the ultimate load of I-columns with 230 section height in this research. A detailed discussion on the length effect is set out in Section 4.2.

421 **Table 7.** Ultimate test loads

Specimen	$N_{u,test}$ (kN)	N_y (kN)	$N_{u,test}/N_y$
H230-690W-L1	2674	2778	0.96
H230-690W-L2	2641	2788	0.95
H230-460W-L1	2458	2449	1.00
H230-460W-L2	2378	2430	0.98
H230-355W-L1	2369	2275	1.04
H230-355W-L2	2302	2273	1.01
H350-690W	2802	3400	0.82
H350-460W	2445	2852	0.86
H350-355W	2371	2598	0.91
H440-690W	2887	3836	0.75
H440-460W	2422	3093	0.78
H440-355W	2363	2788	0.85

422

423 **4 Post-test finite element analysis**

424 To further identify the effect of stub column length and sectional steel combination on the local
425 buckling and post-buckling behaviour of hybrid I-sections with slender web, a post-test finite
426 element (FE) analysis was performed, as presented in this section.

427 **4.1 Finite element models**

428 A software suite-ABAQUS 2019 [32] was utilized to establish numerical models for
429 investigation. Except for the longitudinal displacement at the loaded end, the translational and
430 rotational degrees of freedom for both ends of models were constrained to replicate the

boundary conditions of fixed-ended stub column tests. A 4-node shell element with finite membrane strains-S4R was adopted for element type, and the element size was selected to be equal to half of the plate thickness for balancing the simulation accuracy and computational cost. The true stress-strain relations converted from the measured engineering curves were used for steel materials.

By "BUCKLE" procedure, the first eigenvalue buckling mode under loading condition was taken as the local imperfection shape of I-section, with the magnitude equalling to the measured values in **Table 4**. The study on welding-induced residual stresses for test specimens has been reported by another authors' article [33]. In this research, the measured membrane residual stress results were directly applied to the numerical models.

Taking account of the measured local imperfections and residual stresses, the FE ultimate loads $N_{u,FE\text{-}wrs}$ of specimens are shown in **Table 8**, where the results for models without residual stresses $N_{u,FE\text{-}wors}$ are also tabulated for comparison. Observed from this table, the mean ratios of $N_{u,FE\text{-}wrs}$ and $N_{u,FE\text{-}wors}$ to the ultimate test loads $N_{u,test}$ are 0.98 and 1.03, with the corresponding Coefficient of Variation (CoV) of 0.013 and 0.023, which indicate that both two simulation methods (i.e., with/without the consideration of residual stresses) provide satisfactory predictions for the ultimate load capacity of specimens.

453 **Table 8.** Comparison of ultimate loads between test and finite element results with/without the

454 consideration of residual stresses

Specimen	$N_{u,FE\text{-}wrs}$ (kN)	$N_{u,FE\text{-}wors}$ (kN)	$N_{u,FE\text{-}wrs}/N_{u,test}$	$N_{u,FE\text{-}wors}/N_{u,test}$
H230-690W-L1	2625	2774	0.98	1.04
H230-690W-L2	2564	2748	0.97	1.04
H230-460W-L1	2394	2471	0.97	1.01
H230-460W-L2	2347	2423	0.99	1.02
H230-355W-L1	2271	2328	0.96	0.98
H230-355W-L2	2252	2313	0.98	1.00
H350-690W	2743	2949	0.98	1.05
H350-460W	2427	2571	0.99	1.05
H350-355W	2273	2399	0.96	1.01
H440-690W	2824	3007	0.98	1.04
H440-460W	2421	2561	1.00	1.06
H440-355W	2269	2397	0.96	1.01
Mean			0.98	1.03
CoV			0.013	0.023

455

456 The experimental methods for determining the critical local buckling load presented in Section

457 3.2.1 has demonstrated that the bending strain is a reliable indication of plate buckling.

458 Similarly, the rapid increase of lateral deflection with load is a signal implying that the plate is

459 starting to buckle [6]. In this section, numerical results of the axial load N against web lateral

460 deflection δ_w curve at the mid-length of stub columns for FE models of test series "H230-L1"

461 and "H350", "H440" with and without residual stresses are compared in **Fig. 12**. It is apparent

462 from these figures that the introduction of membrane residual stress decreases the ultimate load
463 capacities of fixed-ended stub columns. This can be explained by that the existence of welding-
464 induced compressive tensile stresses accelerates the buckling as well as plastification within I-
465 sections subject to compression.
466 On the other hand, the impact of residual stresses was found to be similar for all the specimens
467 no matter which web strength grade is adopted. Thus, the numerical method without
468 considering residual stress was utilized in Section 4.3 for analysing the effect of steel strength
469 grade of flange and web plates on the local buckling and post buckling behaviour of slender
470 web I-section stub columns.

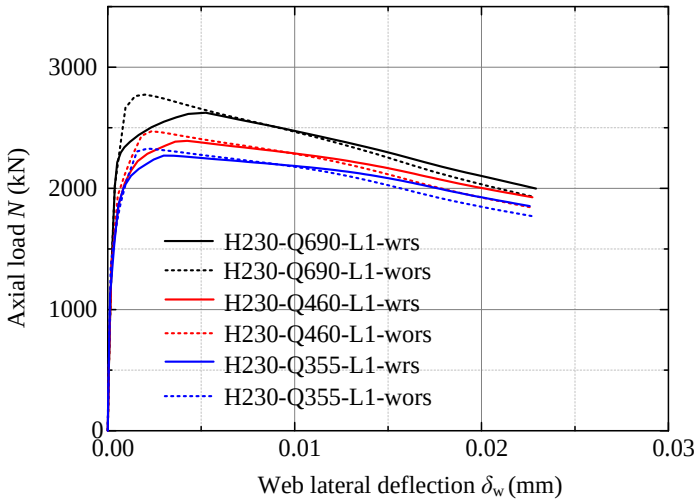

471

472 (a) “H230-L1” series

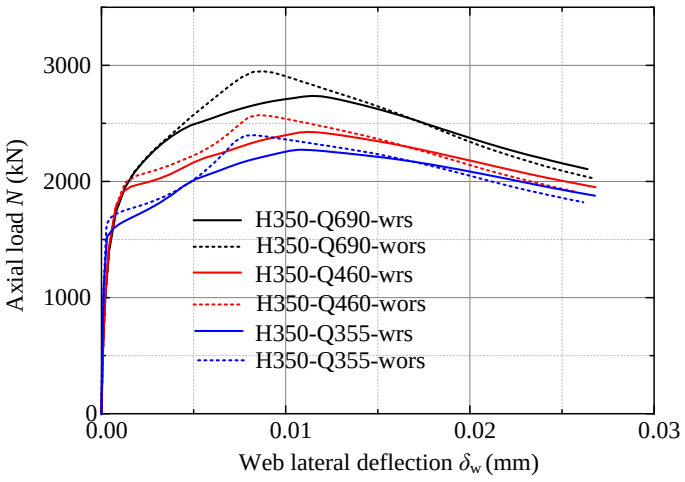

(b) "H350" series

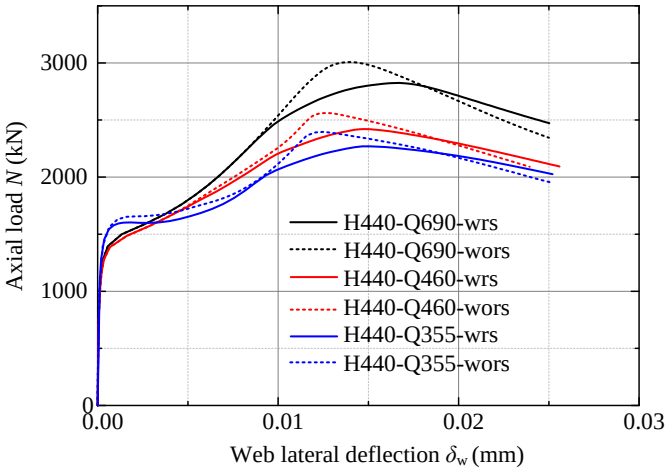

(c) "H440" series

Figure 12. Axial load-web lateral deflection curves at the mid-length of fixed-ended I-section stub columns

4.2 Effect of stub column length

To examine the effect of stub column length on the compressive resistance of hybrid I-sections, on top of the lengths L of $1.2h_w$ and $2.2h_w$ adopted for test specimens, columns with $L=3h_w$ was also investigated in this section. **Fig. 13** shows representative local imperfection shapes for different column lengths. Ultimate load capacities of FE models with member lengths of $1.2h_w$,

485 2.2h_w and 3h_w, denoted by $N_{u,FE-1}$, $N_{u,FE-2}$ and $N_{u,FE-3}$, are compared in **Table 9**. Seen from this
486 table, for "H230" series, the ratio of $N_{u,FE-3}$ or $N_{u,FE-2}$ to $N_{u,FE-1}$ are between 0.96 and 1.00,
487 revealing that L=1.2h_w is able to accurately describe the local buckling behaviour of I-columns
488 with 230 mm section height. For I-sections with 350 mm and 440 mm section heights, it should
489 be noted that flexural buckling occurs in the columns with 3h_w member length. But by
490 comparing $N_{u,FE-2}$ and $N_{u,FE-1}$ of "H350" and "H440" series, it can be concluded that though stub
491 columns with L=1.2h_w receives slight strengthening effect of end restriction, the extent is
492 acceptable, with the ratio of $N_{u,FE-2}$ to $N_{u,FE-1}$ ranging from 0.93 to 0.99. Local buckling failure
493 modes of slender web I-sections with different stub column lengths are illustrated in **Fig. 14**.

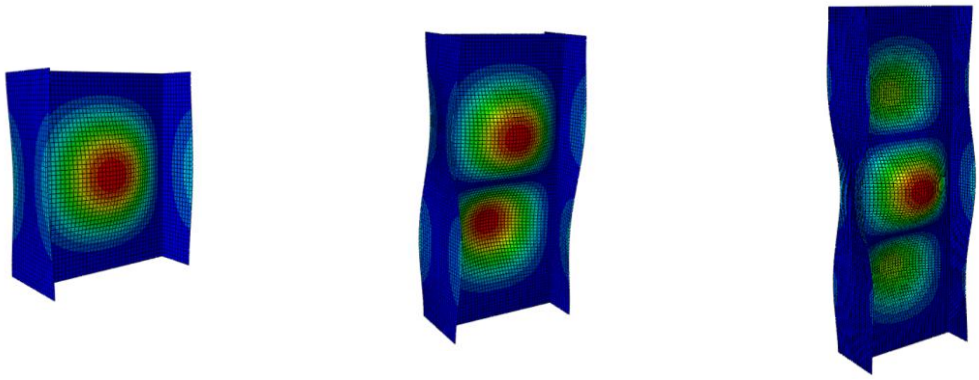

(a) L=1.2h_w (b) L=2.2h_w (c) L=3h_w

494 **Figure 13.** Representative local imperfection shapes of slender web I-sections with different
495 column lengths

496

497 **Table 9**. Numerical ultimate loads of slender web I-sections with different column lengths

Specimen	$N_{u,FE-1}$ (kN)	$N_{u,FE-2}$ (kN)	$N_{u,FE-3}$ (kN)	$N_{u,FE-3}/N_{u,FE\ 1}$	$N_{u,FE-2}/N_{u,FE-1}$
H230-690W-L1	2625	2549	2541	0.97	0.97
H230-690W-L2	2640	2564	2558	0.97	0.97

H230-460W-L1	2394	2299	2304	0.96	0.96
H230-460W-L2	2371	2347	2354	0.99	0.99
H230-355W-L1	2271	2268	2271	1.00	1.00
H230-355W-L2	2259	2252	2256	1.00	1.00
H350-690W	2743	2624	2508[a]	0.91	0.96
H350-460W	2427	2354	2288[a]	0.94	0.97
H350-355W	2273	2243	2185[a]	0.96	0.99
H440-690W	2824	2632	2410[b]	0.85	0.93
H440-460W	2421	2333	2197[b]	0.91	0.96
H440-355W	2269	2215	2107[b]	0.93	0.98

Note: [a] means that the finite element models failed by local-global interactive buckling; [b] means that the finite element model fails by global buckling.

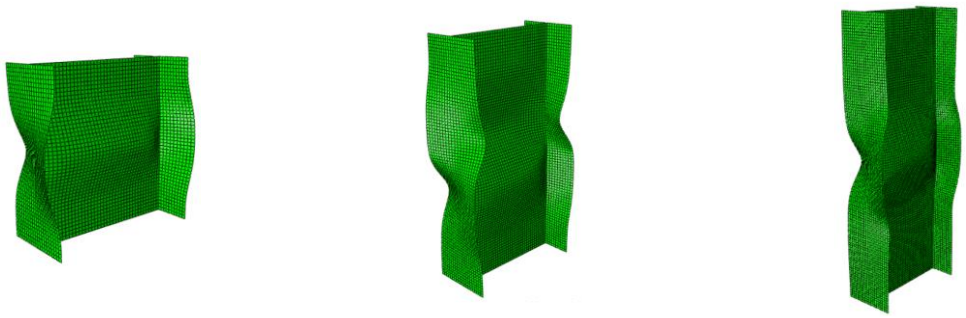

(a) L=1.2h_w (b) L=2.2h_w I L=3h_w

Figure 14. Local buckling failure modes of slender web I-sections with different stub column lengths

4.3. Effect of sectional steel combination

To better understand the effect of flange and web strength grade on the local buckling and post-buckling behaviour of I-sections with slender web, six sectional steel combinations were studied herein, with three groups of nominal cross-section dimensions shown in **Table 2** (i.e., "H230", "H350" and "H440" series). Among them, three are homogeneous sections: "HO-690", "HO-460" and "HO-355" and the other three are hybrid I-sections labelled as specimens "HY-690+460", "HY-690+355" and "HY-460+355". Selection of material for different sectional steel sections is shown in **Table 10**, and the material multi-linear stress-strain relationship used in simulation is based on coupon tensile test results in this research (**Table 3**).

Table 10. Selection of material for different sectional steel combinations

	HO-690	HO-460	HO-355	HY-690+460	HY-690+355	HY-460+355
Flange	Q690-F	Q460	Q355	Q690-F	Q690-F	Q460
Web	Q690-W	Q460	Q355	Q460	Q355	Q355

Note: material characteristics of the selected steels can refer to **Table 3**.

It has been noted in Section 4.1 that the axial load-lateral deflection curve is an effective tool to examine the plate buckling behaviour. In this section, FE models whose local imperfection shapes featured by odd half-wave numbers (i.e., columns with L=1.2h_w and 3h_w) were analysed, so that the lateral deflection of web plate δ_w at the mid-length could capture plate local buckling path efficiently. Note that flexural buckling exists in the failure mode of "H350" and "H440" series with 3h_w length, L=3h_w is only considered for "H230" series.

Fig. 15(a) and **(b)** present the curves of axial load N against web mid-length lateral deflection δ_w for "H230" series with L=1.2h_w and L=3h_w, respectively. As shown in the figures, web strength affects the abrupt transition of N-δ_w curves for 230 mm section height I-sections, which demonstrating the web strength grade governs the onset of plate buckling. This finding confirms the critical local buckling load analysis in Section 3.2 that it is the inelastic buckling that exists in the web plate of "H230" series. Also, by comparing the curves between columns with L=1.2h_w and L=3h_w, it can be found that stub column length shows limited influence on the buckling behaviour, revealing that L=1.2h_w is sufficient to investigate the local buckling and post-buckling behaviour for both homogeneous and hybrid I-sections fail by local buckling. In addition, it was also observed in **Fig. 15** that the growth of axial load capacities after load-deflection transition relies on the flange strength grade. It can be explained by the fact the flange slenderness adopted in the research is stocky enough to experience plastic buckling when reaching load peak.

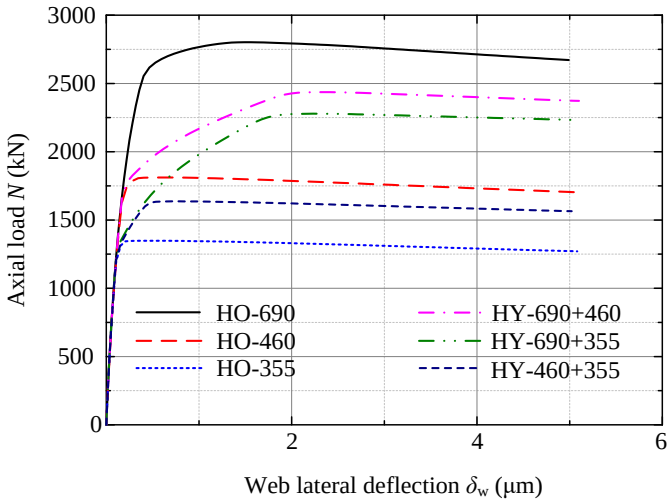

(a) L=1.2h_w

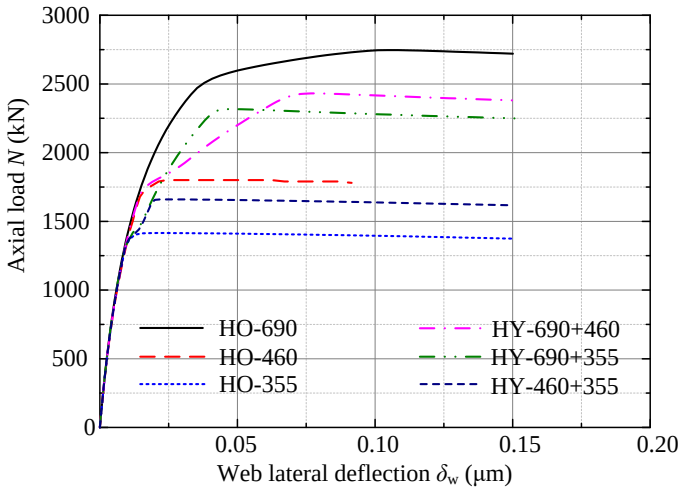

(b) $L=3h_w$

Figure 15. Axial load-web lateral deflection curves for "H230" series

For "H350" series, according to the validated Bleich's equation [31] described in Section 3.2.2, the elastic buckling stress of web plate is 406 MPa, which is slightly higher than the measured Q355 yield strength, but lower than f_y of other steel materials. This result is well reflected by the axial load-web lateral deflection relation of "H350" series in **Fig. 16**: the curve knee point of I-sections with Q355 web (i.e., "HO-355", "HY-460+355" and "HY-690+355" series) are markedly lower than others. For specimens "HO-690", "HO-460" and "HY-690+460", there is no such distinct divergence among curves as which presented by "H230" series, as it is the elastic local buckling, rather than inelastic buckling, occurs in the web plates.

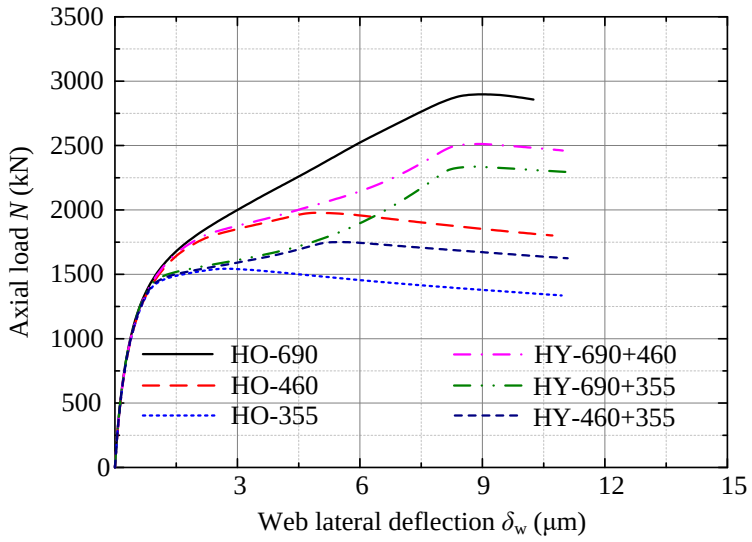

551

552 **Figure 16.** Axial load-web lateral deflection curves for "H350" series

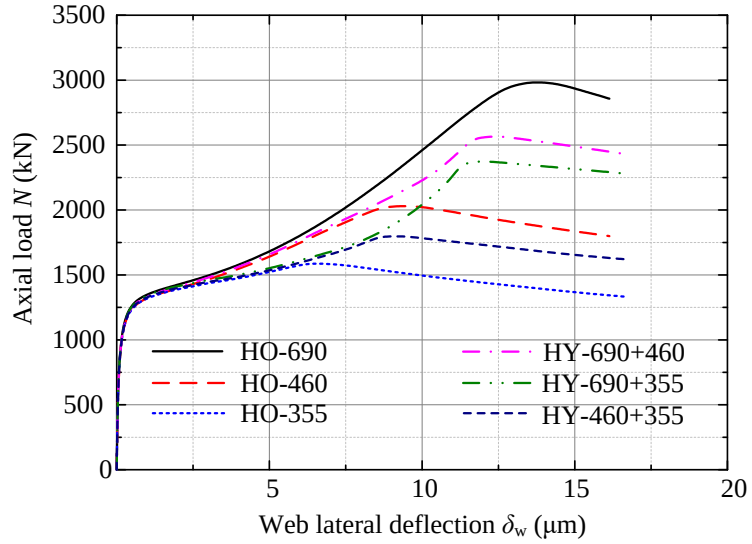

553

554 **Figure 17.** Axial load-web lateral deflection curves for "H440" series

555

556 The axial load N versus web lateral deflection δ_w curves of "H440" series are set out in **Fig. 17**.
557 It can be seen that all the specimens present almost coincident curve knee points, supporting
558 the finding in Section 3.2 that the web plates of specimens "H440" experience elastic local
559 buckling so that the buckling load is independent of steel material. In addition, it was observed
560 from the figure that the web strength grade controls the post-buckling path. In detail, the

increase rate of post buckling strength for “HO-355”, “HY-460+355” and “HY-690+355” is the slowest, whereas that of “HO-690” is the fastest. This phenomenon can be explained by the concept of effective width method: though the central portion of the web plate deflects laterally due to elastic local buckling, whereas the other portions close to the supported edges are constrained to remain straight and continue to carry increasing stresses even after yielding. This idea is supported by the contour plots in **Fig. 18**, which provides the web lateral deflection as well as actively yielding zone for “HO-690” web plate of “H440” series when the column approaches its ultimate load. The actively yielding highlighted in red (**Fig. 18(b)**) demonstrates that there is plastic strain changed during the increment [32]. It is apparent in **Fig. 18(a)** that the web lateral deflection concentrates on the centre of web plate, but it can be seen from **Fig. 18(b)** that except for web centre which going into plasticity due to large deformation, material yielding is also detected near the other portions close to the supported edges.

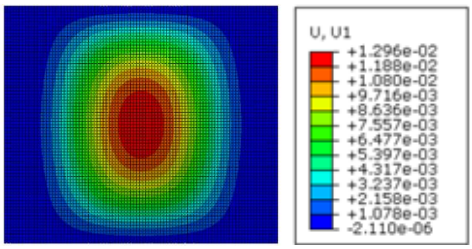

(a) Lateral deflection

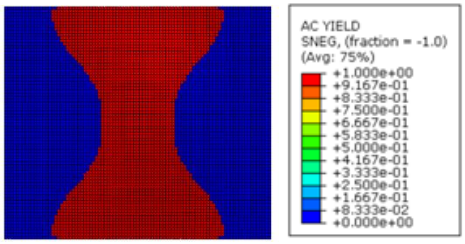

(b) Actively yielding zone

Figure 18. Contour plots for the web plate of “HO-690” in “H440” series

4.4 Summary

Based on the post-test finite element analysis results in this section, it can be concluded that:

(1) For I-sections with slender web investigated in this research, L=1.2h_w is sufficient to capture the local buckling and post buckling behaviour; while L=2.2h_w is the optimal member length for obtaining the most reliable ultimate load capacity of stub columns failed by local buckling;

(2) For I-sections with inelastic local buckling web plate, the web strength undoubtedly affects the compressive strength of stub columns;

(3) For I-sections whose web plate failed by elastic local buckling, web steel grade also plays a non-negligible effect on the ultimate loads of stub columns, indicating that unbuckled portion of web plate still provide the post-buckling strength for I-section stub columns even after yielding.

5 Evaluation of the existing design methods

In this research, the numerical ultimate loads $N_{u,FE-2}$ of fixed-ended stub columns with L=2.2h_w, which are able to rule out the slight strengthening effect of end-restraint as well as the occurrence of global buckling, are used to assess the existing design methods for fixed-ended I-section stub columns with slender web failed by local buckling. The provisions in the Eurocode 3 [14, 34], North American code [9], Australian code [35] and Chinese code [36] for steel structures were firstly investigated. All the above specifications use the effective width method to calculate the design compressive load of isolated plates by introducing a reduction factor. Among these specifications, only Eurocode 3 requires that the classification and effective width of web in hybrid I-section should be based on the yield strength of compression

601 flange [37].

602 The predictions from the Eurocode 3 $N_{u,EC3}$, North American code $N_{u,AISC}$, Australian code
603 $N_{u,AS}$ and the Chinese code $N_{u,GB}$ are compared with the numerical results $N_{u,FE-2}$ in **Table 11**. It
604 is obvious that all the codified design methods make accurate predictions for the ultimate load
605 of tested I-section stub columns. Also, it was found that the least scattered results are given by
606 Eurocode 3.

607 In addition, design expressions of the recently developed DSM and CSM from literatures [7]
608 and [8] are evaluated. Note that the DSM and CSM formulae used herein are derived from the
609 I-sections fabricated by conventional strength steels. Due to the high slenderness of web plate
610 in I-sections, all the test specimens studied in this research are classified into slender cross-
611 sections using DSM and CSM [7,8]. For slender section, the expression of the DSM is indicated
612 by Equation (12), and the CSM ultimate load capacity $N_{u,CSM}$ can be calculated by Equations
613 (13) and (14). In Equation (13), $f_{CSM,f}$ and $f_{CSM,w}$ are the CSM stresses of flange and web, and
614 their values could be determined by Equation (14). It can be seen from Equations (12) to (14),
615 in the DSM and CSM, the flange and web slenderness of I-section is involved in single overall
616 cross-section slenderness λ_p, which may be deficient in describing the cross-section behaviour
617 for sections whose constitutive plates show significantly different buckling performance.

618

619 $$N_{u,DSM} = \left(\frac{0.499}{\lambda_p^{0.465}} + \frac{0.29}{\lambda_p^{0.93}} \right) \times N_y \quad (12)$$

620 $$N_{u,CSM} = A_f \times f_{CSM,f} + A_w \times f_{CSM,w} \quad (13)$$

621 where,

$$\begin{cases} f_{\mathrm{CSM,f}} = f_{\mathrm{yf}} \times \left(1 - \dfrac{0.222}{\lambda_{\mathrm{p}}^{1.05}}\right) \times \dfrac{1}{\lambda_{\mathrm{p}}^{1.05}} \\ f_{\mathrm{CSM,w}} = f_{\mathrm{yw}} \times \left(1 - \dfrac{0.222}{\lambda_{\mathrm{p}}^{1.05}}\right) \times \dfrac{1}{\lambda_{\mathrm{p}}^{1.05}} \end{cases} \quad (14)$$

The accuracy of the DSM and CSM is shown in **Table 11**. It can be seen that the average ratios of the DSM predictions $N_{\mathrm{u,DSM}}$ to the numerical results $N_{\mathrm{u,FE\text{-}2}}$ are 0.90 with the CoV of 0.082, whilst the ones of the CSM results $N_{\mathrm{u,CSM}}$ to $N_{\mathrm{u,\ FE\text{-}2}}$ are 0.88 with the CoV of 0.116. Clearly, compared with the design methods specified in codes, the DSM and CSM experience more scattered predictive results. In detail, for columns belong to "H230" series, both the DSM and CSM present accurate predictions, while I-sections with 350 mm and 440 mm section height, namely, "H350" and "H440" series, worse predictive accuracy is realized by the DSM and CSM. The DSM and CSM curves are compared with test data points in Fig. 19. As seen from this figure, the existing DSM and CSM predictive equations for slender sections underestimate the compressive resistance of both HSS and hybrid I-sections with slender web tested in this research.

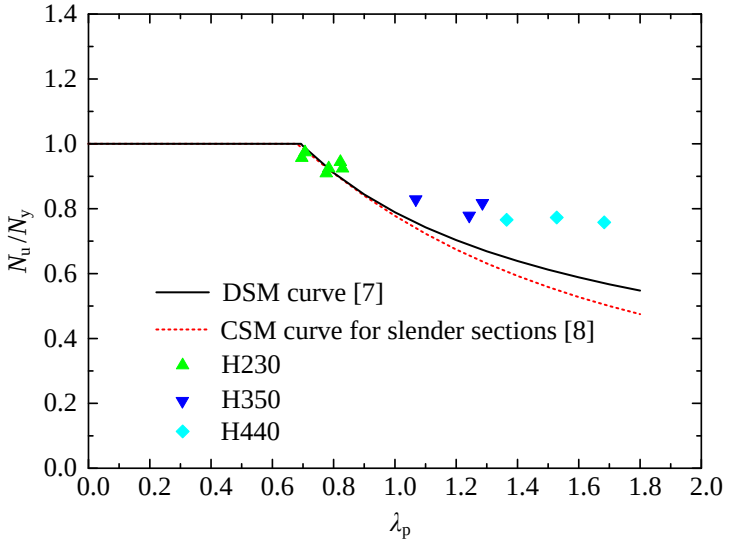

Figure 19. Comparison of DSM and CSM curves with test data points

Table 11. Comparison of the ultimate load between numerical results and existing design methods

Specimen	$N_{u,EC3}$ /$N_{u,FE-2}$	$N_{u,AISC}$ /$N_{u,FE-2}$	$N_{u,GB}$ /$N_{u,FE-2}$	$N_{u,AS}$ /$N_{u,FE-2}$	$N_{u,DSM}$ /$N_{u,FE-2}$	$N_{u,CSM}$ /$N_{u,FE-2}$
H230-690W-L1	0.99	1.01	0.99	0.93	0.97	0.97
H230-690W-L2	1.00	1.00	0.99	0.93	0.97	0.97
H230-460W-L1	0.98	1.02	1.02	0.97	0.97	0.97
H230-460W-L2	0.95	0.98	0.98	0.94	0.94	0.94
H230-355W-L1	0.96	1.01	1.00	0.98	1.00	0.99
H230-355W-L2	0.96	1.01	1.01	0.99	1.00	0.99
H350-690W	1.00	1.02	1.00	0.90	0.87	0.83
H350-460W	0.96	1.02	1.00	0.93	0.81	0.77
H350-355W	0.99	1.07	1.06	1.00	0.88	0.86
H440-690W	1.00	1.01	0.99	0.89	0.83	0.74
H440-460W	0.99	1.05	1.04	0.96	0.80	0.73
H440-355W	0.99	1.07	1.07	0.99	0.82	0.76
Mean	0.98	1.02	1.01	0.93	0.90	0.88
CoV	0.020	0.026	0.027	0.036	0.082	0.116

6 Conclusions

The objectives of this research are to investigate the local buckling and post-buckling behaviour of hybrid I-section stub columns with slender web, which contributes to a better understanding of cross-section behaviour for hybrid I-section under complex scenarios.

Tensile coupon tests and initial local geometric imperfection measurement were conducted,

644 and a total of twelve fixed-ended I-section stub column tests were carried out. The failure mode
645 of stub columns was reported, followed by the experimental and theoretical investigation of
646 the critical buckling load of plate elements for test-specimens, and the ultimate test loads were
647 presented. Furthermore, a post-test finite element analysis was performed to examine the
648 effects of stub column length and sectional steel combination on the local buckling and post
649 buckling behaviour of slender web I-sections under pure compression.
650 Based on the results of experiments and post-test finite element analysis, it was observed that
651 for I-section stub columns whose web plate failed by elastic local buckling, the web strength
652 grade affects the ultimate test loads of test specimens, which indicating that unbuckled portion
653 of web plate still provide the post-buckling strength for I-section stub columns even after
654 yielding.
655 In addition, the applicability of the existing design methods to fixed-ended hybrid I-section
656 stub columns was also assessed underpinned by the validated numerical results. By comparing
657 the existing design methods with the numerical ultimate loads, it was found that the Eurocode
658 3 gives the less scattered predictions than the North American code, Australian code, and
659 Chinese code. Also, it was found that the results from the existing direct strength method (DSM)
660 and continuous strength method (CSM) are more scattered than codified design method, as the
661 existing DSM and CSM predictive equations for slender sections underestimate the
662 compressive resistance of both HSS and hybrid I-sections with slender web.
663 A parametric study covering wider range of both flange and web slenderness is going to be
664 carried out in the future work to understand the local buckling and post buckling behaviour of
665 hybrid I-section further.

Acknowledgements

The support from the Chinese National Engineering Research Centre for Steel Construction (Hong Kong Branch) at The Hong Kong Polytechnic University is gratefully acknowledged. The authors would also like to thank the technical staff, Mr. C. F. Cheung, Mr. M. C. Ng and Mr. K. L. Cheung of the Structural Engineering Research Laboratory, and Mr. H.Y. Leung of the Mechanical Workshop at The Hong Kong Polytechnic University for their assistance on the experimental works.

CRediT authorship contribution statement

Shuxian Chen: Investigation, Writing - original draft; *Jun-zhi Liu*: Writing- review & editing; *Tak-Ming Chan*: Writing- review & editing, Supervision, Funding acquisition.

Reference

[1] Chen, J.B., Chan, T.M. and Varma, A.H. (2020) Stub column behavior of cold-formed high-strength steel circular hollow sections under compression. Journal of Structural Engineering. 146(12), 04020277.

[2] Veljkovic, M. and Johansson, B. (2004) Design of hybrid steel girders. Journal of Constructional Steel Research. 60, 535–547.

[3] Ito, M., Nozaka, K., Shirosaki, T. and Yamasaki, K. (2005) Experimental study on moment–plastic rotation capacity of hybrid beams. Journal of Bridge Engineering. 10(4), 490-496.

[4] Shokouhian, M. and Shi, Y.J. (2015) Flexural strength of hybrid steel I-beams based on slenderness. Engineering Structures. 93, 114-128.

688 [5] Wang, C.S., Duan, L., Chen, Y. F. and Wang, S.C. (2016) Flexural behavior and ductility of
689 hybrid high performance steel I-girders. Journal of Constructional Steel Research. 125, 1 – 14
690 [6] Singer, J., Arbocz, J. and Weller, T. (1998) Buckling Experiments: Experimental Methods
691 in Buckling of Thin-Walled Structures: Basic Concepts, Columns, Beams and Plates – Volume
692 1. John Wiley & Sons, Inc., New York.
693 [7] Li, Y.Z. (2014) Extension of The Direct Strength Method to Hot-Rolled and Welded H
694 Profile Cross-Sections. Ph.D. thesis, University of Liège, Belgium.
695 [8] Yun, X., Gardner, L. and Boissonnade, N. (2018) The continuous strength method for the
696 design of hot-rolled steel cross-sections. Engineering Structures. 157, 179-191.
697 [9] American Institute of Steel Construction (2016) Specification for Structural Steel Buildings,
698 ANSI/AISC 360-16, AISC, Chicago, Illinois.
699 [10] Gardner, L. Fieber, A. and Macorini, L. (2019) Formulae for calculating elastic local
700 buckling stresses of full structural cross-sections. Structures. 17, 2–20.
701 [11] Timoshenko, S.P. and Gere, J.M. (1961) Theory of elastic stability. 2nd ed., New York,
702 NY: McGraw-Hill.
703 [12] European Committee for Standardization. (2006) EN 1993-1-3:2006, Eurocode 3:
704 Design of steel structures - Part 1-3: General rules - Supplementary rules for cold-formed
705 members and sheeting. CEN, Brussels.
706 [13] European Committee for Standardization. (2019) ISO 6892-1:2019 Metallic materials-
707 Tensile testing-Part 1: Method of test at room temperature, CEN, Brussels.
708 [14] European Committee for Standardization. (2006) EN 1993-1-5: 2006, Eurocode 3:
709 Eurocode 3- Design of steel structures-Part 1-5: Plated structural elements. CEN, Brussels.

710 [15] Shi, Y.J. and Xu, K.L. (2019) Experimental and analytical study on local buckling behavior
711 of high strength steel welded I-section beams. International Journal of Steel Structures. 19,
712 1171-1190.
713 [16] Gardner, L. and Nethercot, D.A. (2004) Experiments on stainless steel hollow sections—
714 Part 1: Material and cross-sectional behaviour. Journal of Constructional Steel Research. 60,
715 1291–1318.
716 [17] Roorda, J. and Venkataramaiah, K. R. (1982) Analysis of local plate buckling experimental
717 data. 6th International Specialty Conference on Cold-Formed Steel Structures, 1982, November
718 16-17, Department of Civil Engineering University of Missouri-Rolla.
719 [18] Paszkiewicz, M. and Kubiak, T. (2015) Selected problems concerning determination of
720 the buckling load of channel section beams and columns. Thin-Walled Structures. 93, 112–121.
721 [19] Hu, P.C., Lundquist, E.E. and Batdorf, S.B. (1946) Effect of small deviations from flatness
722 on effective width and buckling of plates in compression, NACA TN 1124.
723 [20] Coan, J.M. (1941) Large-deflection theory for plates with small initial curvatures loaded
724 in edge compression. ASME Journal of Applied Mechanics. 18(2), 143-151.
725 [21] Hoff, N.J., Boley, B.A., and Coan, J.M. (1948) The Development of a Technique for
726 Testing Stiff Panels in Edgewise Compression. Proceedings of the Society for Experimental
727 Stress Analysis. 5(2), 14-24.
728 [22] Barbero, E. and Trovillion, J. (1998) Prediction and measurement of the postcritical
729 behavior of fiber-reinforced composite columns. Composites Science and Technology. 58,
730 1335-1341.
731 [23] Southwell, R.V. (1932) On the analysis of experimental observations in problems of elastic

732 stability, Proceedings of the Royal Society of London. Series A. 135, 601-616.
733 [24] Koiter, W.T. (1982) Elastic Stability, Buckling and Post-Buckling Behaviour. In: P
734 Proceedings of the IUTAM Symposium on Finite Elasticity, August 10-15, 1980, Lehigh
735 University.
736 [25] Debski, H., Kubiak, T. and Teter, A (2013) Buckling and postbuckling behaviour of thin-
737 walled composite channel section column. Composite Structures. 100, 195–204.
738 [26] Cintra, G. G., Cardoso, D. C.T. and Vieira, J.D. (2019) Parameters affecting local buckling
739 response of pultruded GFRP I-columns: Experimental and numerical investigation. Composite
740 Structures. 222, 110897.
741 [27] Cardoso, D.C.T. and Togashi, S.T. (2018) Experimental investigation on the flexural-
742 torsional buckling behavior of pultruded GFRP angle columns. Thin-Walled Structures. 125,
743 269 – 280.
744 [28] Budiansky, B. (1974) Theory of Buckling and Post-Buckling Behavior of Elastic
745 Structures. Advances in applied mechanics.14, 1-65.
746 [29] Heijden, A. M. A. van der. (2009) W.T. Koiter's Elastic Stability of Solids and Structures.
747 Cambridge, Cambridge University Press.
748 [30] Ragheb, W. F. (2015) Local buckling of welded steel I-beams considering flange–web
749 interaction. Thin-Walled Structures. 97, 241–249.
750 [31] Bleich, F. (1952) Buckling Strength of Metal Structures. New York, NY: McGraw-Hill.
751 [32] ABAQUS, User Assistance. Dassault Systèmes Simulia Corporation, Providence, Rhode
752 Island, USA.; 2019.

753 [33] Chen, S.X., Liu, J.Z. and Chan, T.M. (2023) Material properties and residual stresses of
754 welded high strength steel and hybrid I-sections. Engineering Structures. 276, 115293.
755 [34] European Committee for Standardization. (2005) EN 1993-1-1:2005, Eurocode 3: Design
756 of Steel Structures-Part 1-1: General Rules and Rules for Buildings, CEN, Brussels.
757 [35] Standards Australia. (2020) AS 4100:2020, Steel structures. AS, Sydney, Australia.
758 [36] Ministry of Housing and Urban-Rural Development of the People's Republic of China.
759 (2017) Standard for the design of steel structures, GB 50017-2017. China Architecture &
760 Building Press, Beijing. (in Chinese)
761 [37] Baddoo, N and Chen, A.Q. (2020) High Strength Steel Design and Execution Guide. the
762 Steel Construction Institute, SCI, UK.